Biophysical Journal
Article

Biophysical Society

The Structural Basis of IKs Ion-Channel Activation: Mechanistic Insights from Molecular Simulations

Smiruthi Ramasubramanian[1] and Yoram Rudy[1,*]
[1]Department of Biomedical Engineering and Cardiac Bioelectricity and Arrhythmia Center, Washington University in St. Louis, St. Louis, Missouri

ABSTRACT Relating ion channel (iCh) structural dynamics to physiological function remains a challenge. Current experimental and computational techniques have limited ability to explore this relationship in atomistic detail over physiological timescales. A framework associating iCh structure to function is necessary for elucidating normal and disease mechanisms. We formulated a modeling schema that overcomes the limitations of current methods through applications of artificial intelligence machine learning. Using this approach, we studied molecular processes that underlie human IKs voltage-mediated gating. IKs malfunction underlies many debilitating and life-threatening diseases. Molecular components of IKs that underlie its electrophysiological function include KCNQ1 (a pore-forming tetramer) and KCNE1 (an auxiliary subunit). Simulations, using the IKs structure-function model, reproduced experimentally recorded saturation of gating-charge displacement at positive membrane voltages, two-step voltage sensor (VS) movement shown by fluorescence, iCh gating statistics, and current-voltage relationship. Mechanistic insights include the following: 1) pore energy profile determines iCh subconductance; 2) the entire protein structure, not limited to the pore, contributes to pore energy and channel subconductance; 3) interactions with KCNE1 result in two distinct VS movements, causing gating-charge saturation at positive membrane voltages and current activation delay; and 4) flexible coupling between VS and pore permits pore opening at lower VS positions, resulting in sequential gating. The new modeling approach is applicable to atomistic scale studies of other proteins on timescales of physiological function.

INTRODUCTION

A voltage-gated ion channel (iCh), in response to membrane voltage (V_m), undergoes atomistic structural changes that are stochastic in nature and underlie its physiological function as a transmembrane (TM) charge carrier. Recent advances in experimental techniques (1) provide considerable structural details that can be used to simulate atomistic structural dynamics. Relating these dynamics to the physiological function of proteins, including iCh, remains a major objective and difficult challenge in the field of biophysics. In principle, computational techniques can be used to simulate structure-based iCh function to explain its mechanism (2,3). However, even with customized hardware, simulations of 1-ms gating dynamics take months and require nonphysiological conditions, e.g., a V_m of 500 mV (4,5).Therefore, direct computation of iCh conformational changes during gating, with atomistic structural details and over a sufficiently long timescale (10s of ms), is impractical.

In this study, we introduce a methodology that utilizes machine learning (ML) for modeling iCh with structural and functional details. The method can be used to probe mechanisms that govern ionic conductance and voltage-mediated gating at sufficient atomistic resolution over physiological timescales. The protein archetype we chose is the slow delayed rectifier IKs, a human voltage-gated potassium iCh. IKs is composed of a KCNQ1 pore-forming tetramer modulated by KCNE1 segments. It plays an important role in cardiac action potential (AP) repolarization during β-adrenergic stimulation and participates in cardiac AP-rate-dependent adaptation (6,7). IKs mutations are implicated in the most common congenital long QT syndrome, Type 1, and in severe neurological disorders such as deafness and epilepsy (8). Additionally, this channel poses many structure-function molecular properties of interest, such as multiple subconductance (SC) levels, two distinct gating conformational movements, voltage sensor (VS) or S4 movement that precedes ionic current, gating-charge (GC) saturation at positive V_m, and sequential gating (9–11). The new ML-based modeling approach simulates experimental data with high accuracy and reproduces these properties; it provides mechanistic insights on

Submitted February 7, 2018, and accepted for publication April 13, 2018.
*Correspondence: rudy@wustl.edu
Editor: Eric Sobie.
https://doi.org/10.1016/j.bpj.2018.04.023

the molecular basis of iCh activation under physiological conditions.

METHODS

A short overview of simulating structural dynamics and electrophysiological function is provided below; details are included in the Supporting Materials and Methods. The energy landscape was constructed to simulate IKs structural changes in response to V_m. If done explicitly, this process requires computing the energy of all possible IKs conformations. This is an impossible task given the vast number of degrees of freedom. Previous modeling overcame these difficulties by retaining only large backbone movement with limited degrees of freedom, assuming tetrameric symmetry and reducing simulations to KCNQ1 TM segments (12–15). Here, we apply ML to simulate physiological IKs behavior at the atomistic scale, without the approximations and simplifications of previous work.

Structure to function

The initial IKs structure was constructed from experimental data using computational modeling (Fig. 1); the specifics are detailed in the Supporting Materials and Methods. Extensive de novo sampling of IKs conformational space (library: ~3,000,000 conformations) was performed without any dimension reduction, applying physiological and experimental constraints. MODELLER (16) was used to minimize energy and remove steric clashes. Selected IKs attributes (features) that alter protein energy were extracted from the library, along with the computed energy of each corresponding structure (17,18). Using these data, the ML algorithm (19) was trained to predict IKs energy of structures outside the library. With this approach, the energy landscape covered the entire IKs conformational space associated with activation. If desired, the structure for any point on the energy landscape could be retrieved. CHARMM force fields were used for energy calculations (20).

Multidimensional random walks (with Metropolis-Hastings criterion (21)) on the energy landscape at different V_m quantified the transition probability between different regions of the energy landscape. The time step of the simulated random jumps was estimated from experimentally obtained single-channel kinetic data (9) (~0.17 ms). Note that jump resolution could be as small as 10^{-12} steps, and the maximal allowed structural deviation between jumps was 1 Å. The structures visited in the random walks were clustered in two physiological dimensions of interest: Avg.S4Z (average Z position of four VS in the tetramer) and PD (the minimum pore diameter at the activation gate). Conformational jumps between structure pairs from random walks were used to construct the transition matrix of structural clusters (Supporting Materials and Methods). All simulations were conducted at room temperature (21°C), consistent with experiments. Note that PyMOL (22) was utilized for all protein visualizations.

Calculating SC using IKs pore energy

To simulate IKs function (e.g., single-channel and macroscopic current) starting from simulated structural changes during gating, each structure cluster SC was calculated. A representative structure for each cluster was used to calculate the energy profile (using particle mesh Ewald (23)) across the membrane in the pore region (Fig. 2 *A*). This pore-energy profile (energy barrier) of the representative IKs would affect the probability of an ion passing through the pore (P_{ion}). The peak of the energy barrier (located at the activation gate) was used to construct the pore-energy map (Fig. 2 *A*, *center*). This map was used to obtain parameters f (an

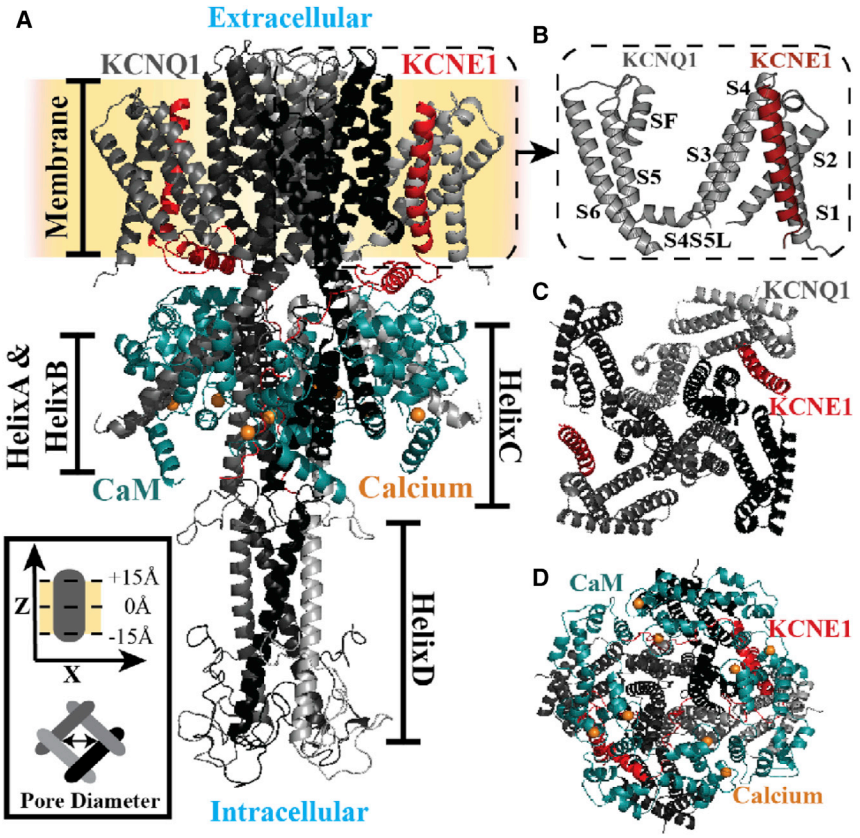

FIGURE 1 IKs structure. (*A*) A side view of initial IKs structure (KCNQ1 tetramer bound to two KCNE1) is shown. CaM is bound to HelixA&B and is proximal to the KCNE1 cytoplasmic helix. The KCNE1 intracellular segment interacts with HelixC's dimer-of-dimers, and the HelixD tetramer binds with Yotiao (protein not shown) to facilitate IKs phosphorylation. In addition, HelixC and HelixD are suggested to play a role in subunit dimerization and tetramerization, respectively (26). The inset (*bottom left*) shows the coordinate system of IKs (*gray*; *side* and *bottom* views) in the membrane (*yellow*). (*B*) An expanded view of the TM S1–S6 arrangement is shown. (*C*) A top view (without CaM and KCNQ1 C-terminus) and (*D*) bottom view of IKs are shown. The structural components and identifying symbols are color coded. S4S5L, S4-S5 linker; CaM, Apo-Calmodulin.

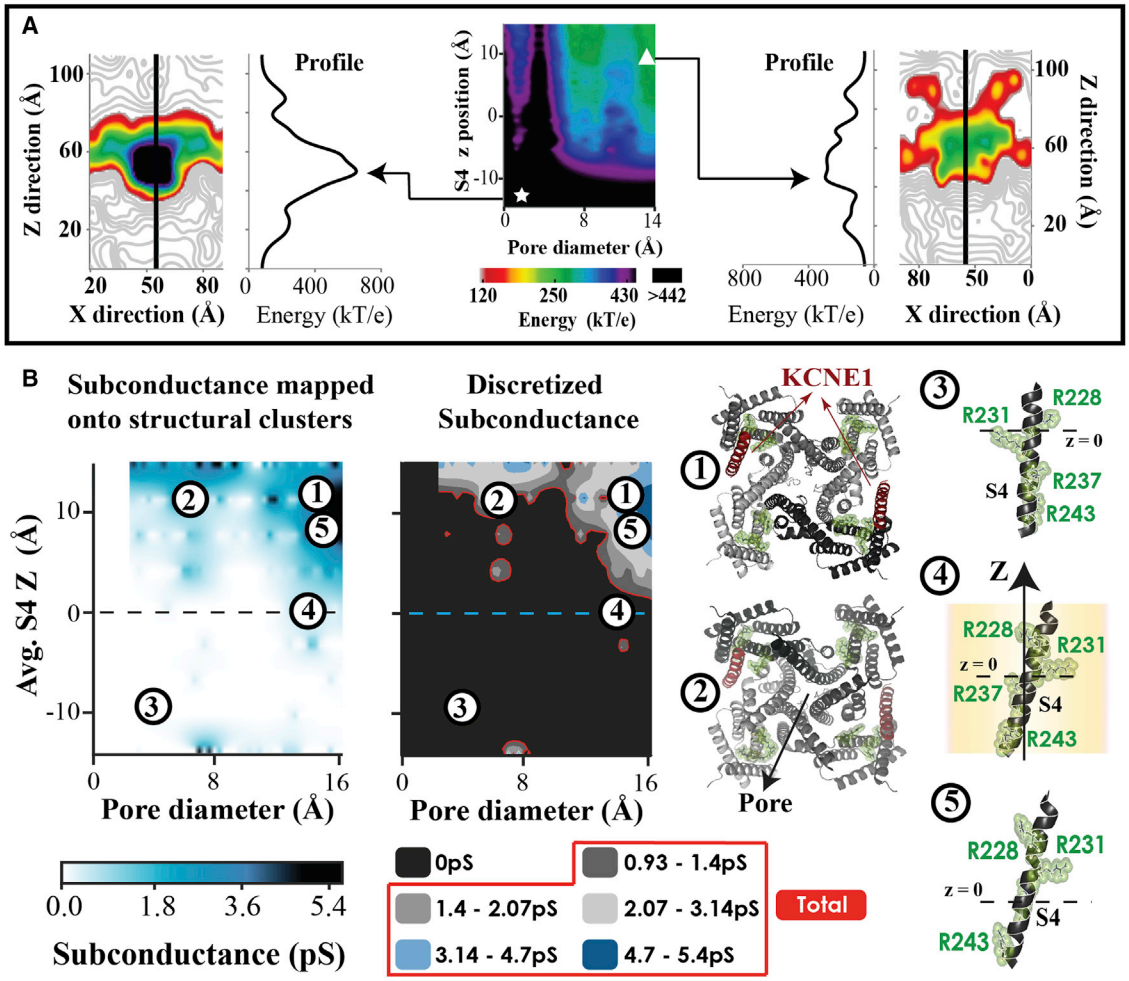

FIGURE 2 Structure-based SC computed from pore energy profile. (*A*, *center*) The largest IKs energy barrier across the pore is projected on a two-dimensional conformational cluster map (PD and Avg.S4Z position). The symbols indicate representative structures from two different clusters: low S4 *Z* position and small pore (*white star*), and high S4 and large pore (*white triangle*). Corresponding pore energy maps (*X-Z* slice) for these structures are shown together with the energy profile across the membrane along a center line (*black*). (*B*) The calculated SC values from the pore energy barrier are projected on a two-dimensional (PD and Avg.S4Z) conformational cluster map (SC map, *left*). The estimated SC are grouped into five discretized conducting levels based on experimental measurements (9) (SC map, *right*). The total conductance (*red*) is used to simulate macroscopic current and calculate single channel statistics (Supporting Materials and Methods). Protein structures in relation to SC are shown in the right panels. They depict representative pore (*bottom view*) and S4 (*side view*) structures from selected clusters on the map. Positively charged S4 residues (R228, R231, R237, R243) are identified (*green*). Numbers indicate structure locations on the SC map. Only one of four possible S4 conformations is shown.

energy-barrier-scaling constant used to account for extrinsic factors that affect ion conduction) and G_{max} (maximal conductance) of Eqs. 1 and 2, using experimental data (9,24). A Boltzmann distribution for pore energy (E) was assumed, and a self-adaptive differential evolution algorithm (25) was used to estimate SC in Eq. 2. The ionic current (I_K) (Eq. 3) was calculated based on SC and number of ion channels in cluster i (N_i), with the reversal potential (E_K):

$$P_{ion_i} = e^{(-E_i \times f)}, \tag{1}$$

$$SC_i = G_{max} \times P_{ion_i}, \tag{2}$$

and

$$I_K(t) = \sum_i SC_i \times N_i(t) \times (V_m - E_K). \tag{3}$$

G_{max} and f were estimated to be 1.9e9 S and 9.31e−2 kT/e, respectively. SC was assumed to be conformation-specific and the same at all V_m, because pore-energy profile changes due to V_m changes were negligible. A flowchart of simulation steps (Fig. S7) and details on specific gating mechanism calculations are provided in the Supporting Materials and Methods.

RESULTS

An IKs structure (Fig. 1) was constructed using available experimental data (26) and homology to Kv1.2/2.1 (Supporting Materials and Methods). Although it was not assumed that S3 and S4 move together, conformations in the library indicate that S3 moves and rotates to accommodate S4 upward movement during gating; this is expected, as the segments are tightly coupled by a short linker. The

KCNE1 TM segment also moves and rotates to accommodate S4 conformational changes.

Structural basis of SC and simulated ionic currents

The pore-energy barrier depends on IKs structure. The *Z*-profile of pore energy (Fig. 2 *A*) has a large barrier for ions to cross at the pore activation gate. However, this barrier is lower for structures with high Avg.S4Z and large PD (Fig. 2 *A*, *white triangle*). These clusters, with lower energy barriers, have a greater probability of ions passing through the pore as compared to structures with low Avg.S4Z and small PD (Fig. 2 *A*, *white star*). Consequently, they are associated with higher SC levels and greater ionic current. Fig. 2 *B* shows the calculated SC map computed from the pore-energy map (Fig. 2 *A*, *center*). Structure clusters with the lowest energy barrier (Fig. 2 *A*, *white triangle*) have large PD and high Avg.S4Z; they also have the highest estimated SC (Fig. 2 *B*; clusters 1 and 5). As such, SC is dependent on PD as previously suggested (27). Additionally, VS conformational changes and associated IKs structural changes also affect SC.

The estimated SC map (Fig. 2 *B*) was used to simulate IKs function as a current carrier. The simulated function was compared to experiments under similar conditions and voltage protocols (9) (Fig. 3, *A–E*). Simulated single-channel current traces and the macroscopic current (average of 100 such traces) showed good correspondence with experimental data (Fig. 3, *A* and *B*). SC levels, accessed during activation upon step depolarization to 60 mV from −80 mV, were equivalent to experimental measurements (Fig. 3 *C*). The simulated mean single-channel current amplitudes at different depolarized V_m were used to calculate the microscopic current-voltage (I-V) relationship; an example calculation at 60 mV is shown in Fig. 3 *D*. The I-V curve shows excellent correlation with experimental recordings (Fig. 3 *E*). Similar to experiments, simulations showed many silent single-channel traces for which IKs structural changes did not result in conducting pore conformations. Simulated single-channel latency to first opening during a step depolarization to 60 mV was 1.65 ± 0.08 s (Supporting Materials and Methods), consistent with the experimental value (1.67 ± 0.008 s, for the current amplitude of 0.5 pA). Relevant single-channel current characteristics such as total dwell time, mean open time, and first opening probability were calculated for each SC level at different V_m (Figs. S15 and S16). Simulated single-channel traces showed increased access to higher SC levels with larger depolarizing V_m.

Two distinct VS movements

Simulated structural changes, associated with VS movement during depolarization (at different V_m), were consistent with the results of fluorescence experiments (10). Analysis of 2000 IKs trajectories identified two possible VS movements at negative and positive V_m (Fig. 4). Upon depolarization, VS underwent an initial fast ~9 Å upward *Z* movement, followed by a slower ~2 Å movement (maximal Avg.S4Z translation at steady state (SS)). The rate of accompanying PD increase was slow compared to Avg.S4Z translation (Fig. 5). Simulated S4 *Z* movement preceded ionic current, consistent with experiments (10). SS occupation of structural states at −80 mV (holding potential, HP) identifies three IKs conformational clusters (HPSS clusters) likely to

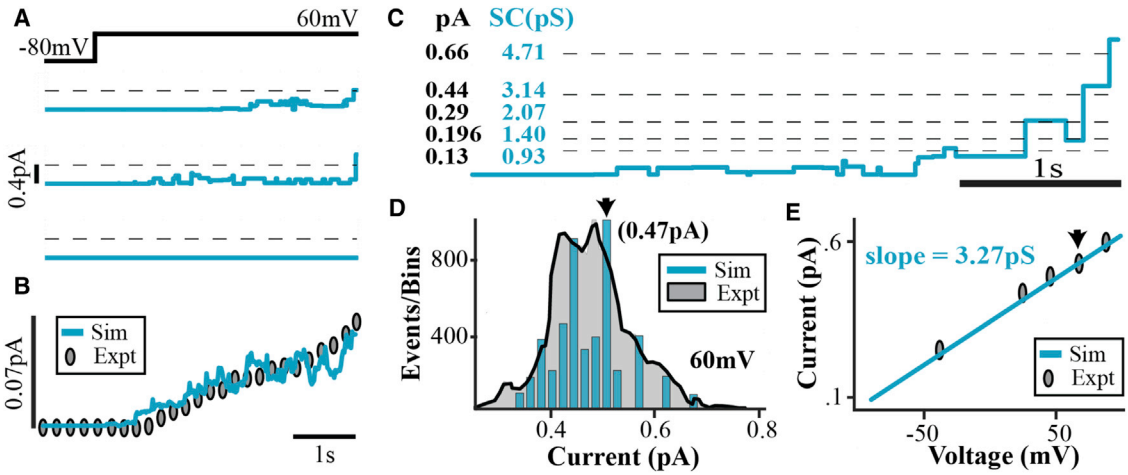

FIGURE 3 (*A*) Three simulated single-channel current traces for a step depolarization V_m from −80 to 60 mV. (*B*) The ensemble current (average of 100 traces) fits the experimental data (9). (*C*) An expanded section of a simulated single-channel trace is presented here. Experimentally identified current levels (9) (*dashed lines*, *black entries*) and SC computed from simulations (*blue entries*) are shown. (*D*) A current amplitude histogram of simulated single-channel traces at 60 mV (*blue*) and the corresponding experimental data (*shaded gray*) (9) is given. The arrow indicates the mean current amplitude histogram (0.47 pA, also indicated by the arrow in (*E*)). (*E*) Similar histograms (to (*D*)) are constructed for a range of V_m to obtain the microscopic I-V relationship (*blue line*) that fits experimental data (*symbols*) with a slope (mean conductance) of 3.27 pS (as determined experimentally (9)).

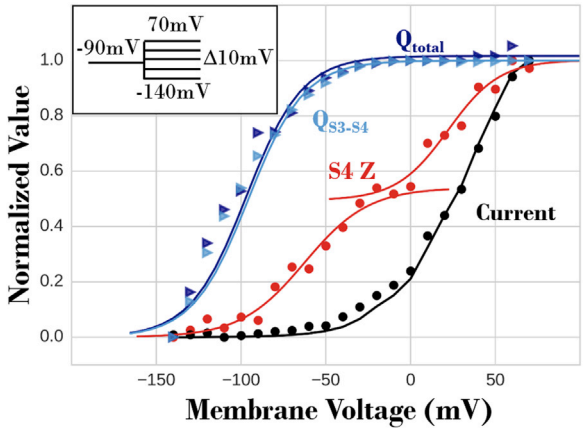

FIGURE 4 GC displacement (*blue*), S4 *Z* (*red*), and macroscopic current (*black*). Normalized simulated current (*black circles*) and the sum of tetramer S4 *Z* displacements (*red circles*) in 2000 iCh, 4 s past depolarization (for the protocol in the *inset*), are given. The black line represents experimental data (24). The S4 *Z* data are fitted with two sigmoidal curves at negative and positive V_m, representing the I and II movements of S4, respectively. At positive V_m, an increasing fraction of S4 in the 2000 iCh transitions to the II movement. GC displacement associated with one representative iCh S4 *Z* transition is calculated based on two selections: the entire IKs (Q_{total}, *dark blue*) and S3-S4 segments only (Q_{S3-S4}, *light blue*) at different V_m. The GC data are fitted with a single sigmoid (*light* and *dark blue traces*), analogous to the S4 *Z* data at negative V_m.

transition to conducting conformations upon depolarization (Fig. 5, *right-top*, *blue*, *green*, *pink symbols*). Three likely pathways between HPSS clusters and high SC cluster (Fig. 5, *right-top*, *black symbol*) were ascertained for 60 mV step depolarization. The temporal probability of each pathway (Fig. 5, *right-middle*) showed that conformations with large pore at −80 mV transition faster to high SC conformations (large PD, high Avg.S4Z) than conformations with a smaller pore. Fig. 6 provides a summary and schematic representation of S4 and pore conformational changes during activation.

Important residue-pair interactions that affected VS conformational changes were identified by calculating their contribution to IKs structural energy (Fig. S17). There are two S4 positions relative to KCNE1, proximal and distal (Figs. 1 *C* and S17). Proximal S4 charged residues interacted strongly with charged residues at the bottom of the KCNE1 segment (Fig. S17 *C*). In contrast, two distal S4 charged residues were only weakly influenced by KCNE1 (Fig. S17 *B*). These differences resulted in two types of VS *Z* movement of proximal S4 and distal S4, respectively. Residue-interaction-energy computations (Fig. S17) show stabilization of distal S4 at *Z* position 1.44 Å and of proximal S4 at 1.44 and 2.88 Å. In addition, proximal S4 shows strong stabilization at −6.75 and −4.44 Å and increasing stabilization between 0.33 and 2.88 Å. These different stabilization profiles (Fig. S17, *B* and *C*; *bottom panel*) suggest that distal S4 undergoes a single fast *Z* movement to its stabilized high *Z* position, whereas proximal S4 experiences two movements—a slower *Z* translation to about −2.78 Å, followed by a faster upward *Z* movement to ∼3 Å. It follows that distal S4 contributes mostly to the initial fast and large *Z* translation (to ∼1 Å), and proximal S4 is responsible for the additional slower S4 *Z* movement (to ∼3 Å) at positive V_m, resulting in more conformations transitioning to high SC clusters.

GC saturation and sequential gating

The model also replicated the experimentally observed saturation of GC displacement at positive V_m (Fig. 4). This property is the result of the two aforementioned VS *Z* movements—at negative V_m, the VS underwent a fast and large *Z* translation with large charge displacement, and at positive V_m it experienced an additional slow and small *Z* translation (Fig. 6) that contributed very little to GC displacement. GC calculations with only S3–S4 segments (Q_{S3-S4}) and with the entire protein (Q_{total}) showed that S3–S4 movement contributes most to GC displacement. Using alternative structural clustering (Supporting Materials and Methods), all possible combinations of S4 *Z* movements in the tetramer were suppressed, and macroscopic current (2000 IKs channels) at the end of 4-s step depolarization was recorded (Fig. 7). Ten simulations were conducted for each combination of immobilized S4, and the resulting currents were normalized to control (IKs current with all four S4 mobile). If S4 movements were cooperative and required concerted transitions during gating, then the immobilization of S4 would have resulted in zero current. However, Fig. 7 shows that current decreases linearly with an increased number of immobilized S4, consistent with experimental data (11). This linearity confirms independent S4 movement and shows that each S4 contributes incrementally to IKs gating.

SC validation

In addition to computing SC from simulated pore energy (Fig. 2 *B*), SC was estimated from fitting experimental data (Fig. S18). The estimated SC map was used to simulate macroscopic current, microscopic current, and I-V relationships (Fig. S18, *A–D*) with high accuracy relative to experiments (9,24); the SC map from experimental data (Fig. 18 *E*) was extremely similar to the SC map calculated from pore energy (Fig. 2 *B*), with analogous locations of high SC clusters and nonconducting clusters.

DISCUSSION

Experimental techniques that visualize atomistic structural dynamics (28) are difficult to utilize with large IKs proteins, because they contain multiple domains with flexible regions. Molecular dynamics simulations provide valuable data on a possible structural pathway between two known iCh conformations (endpoints) on the millisecond

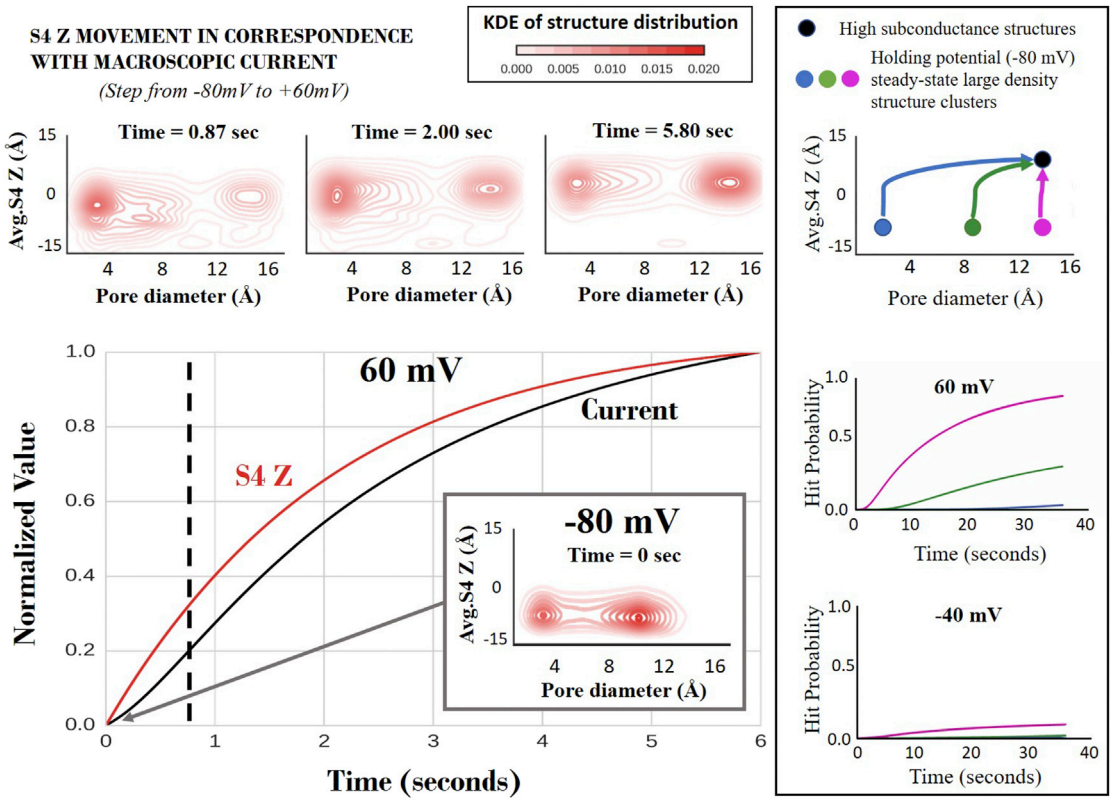

FIGURE 5 Two movements of the voltage sensor and pore. (*Center*) The normalized S4 *Z* movement and macroscopic current (2000 ion channels), calculated for a depolarizing potential to 60 mV from a holding potential of −80 mV, show that the S4 movement in the *Z* direction precedes ion conduction through the pore. The dashed line divides approximately the two time courses of major conformational changes between structure clusters shown in the right panel. (*Top*) The KDEs calculated based on the temporal occupancy of the structure clusters are shown at the top for three different times. Comparing the structure-cluster KDE at −80 mV holding potential (*center panel* (*inset*)) and 0.87 s after 60 mV depolarization, it can be seen that the initial movement of S4 in the *Z*-direction (∼9 Å) is fast. As time progresses (at 2 and 5.8 s), the S4 *Z* moves slower to a slightly higher *Z* position (∼1.4 Å, at 6 s) with high conductance. The pore opening from a small to a large pore diameter is also much slower than the initial S4 movement. (*Right*) The top panel identifies major cluster structures occupied at a holding potential of −80 mV (*pink*, *green*, and *blue filled circles*). They correspond to the KDE map at −80 mV (*center panel*), except the pink clusters do not show on the map scale. The colored arrows mark the most probable trajectories of the structures to the high SC clusters (*black filled circle*) during application of a depolarizing potential. The middle and bottom panels show the time progression of the probability of these trajectories (*color coded*) for two different membrane potentials, +60 mV (*middle*) and −40 mV (*bottom*).

timescale. Because single-channel dynamics are stochastic, extensive IKs structural changes occur between closed and open states as a function of V_m and time, ensuing in multiple transition pathways over a millisecond-to-second timescale. Therefore, multiple endpoints molecular dynamics computations are not viable on a physiological timescale (5,29). Previous structure-based functional models did not account for SCs because a single-conductance concerted or allosteric constraint was assumed to simulate current (12–15). Knowledge of an experimentally resolved static iCh structure, although insufficient to decipher global structural dynamics, provides a plethora of information (e.g., secondary structure propensities, flexible regions, connectivity, etc.) to build a library of possible gating conformations at the required atomistic resolution (Methods and Supporting Materials and Methods). Many of our library IKs conformations (sans KCNE1) were found with small deviations from the recently published electron cryo-microscopy (cryo-EM) KCNQ1 structure (Fig. S11).

The ML algorithm (19) used to construct the multidimensional protein energy landscape converged and was able to predict IKs structural energy with negligible error (Supporting Materials and Methods). This approach circumvented the impossible computation of constructing all possible IKs structures. To correlate the simulated structural transitions to experimentally measured ionic current, the partition function of the computed energy landscape was obtained from IKs single-channel kinetics (9). Library IKs structural energy shows that electrostatic energy contributes overwhelmingly to the total energy (Supporting Materials and Methods; Figs. S12 and S13). As a result, changes in IKs energy due to V_m can be adequately represented by changes in electrostatic energy. The simulated structural and functional changes were validated using independent experiments, other than those used for parameter estimations; the IKs model reproduced the recordings of ensemble structural changes, ionic current characteristics, and I-V relationships (10,11,24).

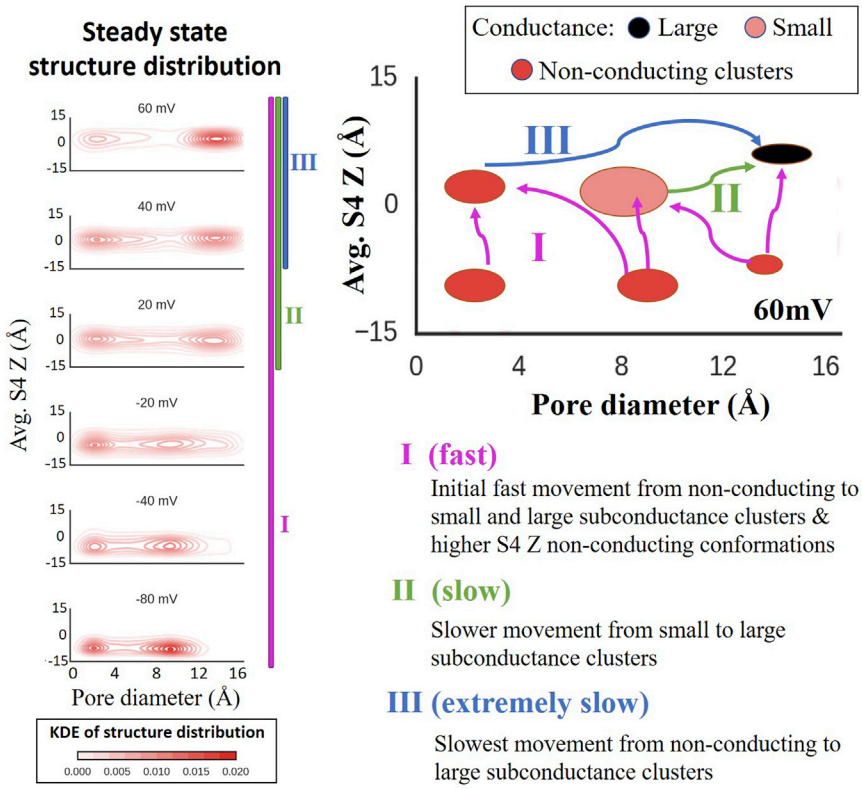

FIGURE 6 Fast and slow movements of the S4 in *Z* direction and pore opening. (*Left*) The steady-state structure cluster KDE for the indicated V_m when depolarized from the holding potential of −80 mV is shown. These panels represent transitional structure distributions when a step voltage of 60 mV is applied from a holding potential of −80 mV. The comparison of the temporal KDE plots (Fig. 5, *top*) with the steady-state KDE (*left*) indicates that at negative V_m, only the first fast transition (I) occurred, whereas at positive V_m, the first transition followed by a slower second transition (II) was observed. The first transition captures the major movement of the S4 in the *Z* direction, after which the second transition only shows a slight increase in the S4 *Z* (∼1.4 Å) and is consistent with the gating charge calculations shown in Fig. 4. The slowest transition (III) contributes very little to the current and conformational changes observed in the simulation time course. (*Right*) Cartoon schema of the fast, slow, and extremely slow conformational changes. The pink arrows represent the initial fast conformational transition because of S4 movement in the *Z* direction, whereas the green arrow shows the slower transition from medium to large pore and the further small S4 *Z* movement. The blue arrow represents the extremely slow transition from a very small pore to a large pore. Note that the observed transitions are not sequential and happen simultaneously.

IKs structure-based SC determination

IKs structural changes in response to V_m depolarization were simulated, and the corresponding function (ionic current) was calculated by associating a pore conductance to a structure cluster. Gating conformations with S4 at higher *Z* have lower energy barriers at the pore activation gate. This is because the repulsive electrostatic field in the pore, influenced by the four positively charged S4 segments (tetramer), is mitigated by the shielding effect of the surrounding protein segments and water at higher S4 *Z* positions. Therefore, conformations with low or high S4 *Z* positions have low or high SC levels, respectively. In addition, SC levels are also affected by PD.

The pore-energy profile was computed in the absence of explicit K^+ ions in the pore. This permitted us to calculate SC as an intrinsic property of IKs, independent of extrinsic factors that affect ion conduction such as number, location, and hydration characteristics of pore ions. Therefore, SC computations are based solely on the IKs molecular structure and its propensity to allow ionic conduction. With these properties, the model correlates structural changes to functional observations and replicates experimentally observed IKs characteristics, including five discrete SC levels (between 0.13 and 0.66 pS (9)).

Analysis of early IKs single channel recordings showed a four-times-larger conductance as compared to KCNQ1 (24,30). It also displayed a strong Cole-Moore effect, i.e., activated VS did not result in immediate current. It was suggested that this difference could be due to KCNQ1's ability to access multiple SC states, whereas IKs could only access the largest SC state during activation (31). However, IKs and KCNQ1 do not have access to the same SC states during VS activation. In the absence of KCNE1, the structure-based SC map of KCNQ1 changes significantly. Without the mitigating effect of negatively charged KCNE1 residues, the energy barrier across the KCNQ1 pore is larger for high-S4-*Z* and wide-pore KCNQ1 conformations. In the absence of KCNE1, we anticipate that KCNQ1 S4 will behave similarly to distal S4 of IKs and will not have the II S4 movement (that allows access to larger SC states; Fig. 6). With this information, we envision that both KCNQ1 and IKs conduct ionic current at multiple SC levels, and we further predict that the KCNQ1 SC range will be three to four times smaller than that of IKs. It follows that, for every addition of KCNE1 to KCNQ1, larger SC states will be accessible by the iCh.

S4 movement precedes ion conduction through the pore

Fluorescence experiments provide data on S4 movement during channel gating. However, this technique cannot quantify the exact S4 movement. Also, depending on the probe utilized, fluorescence intensity measurements can

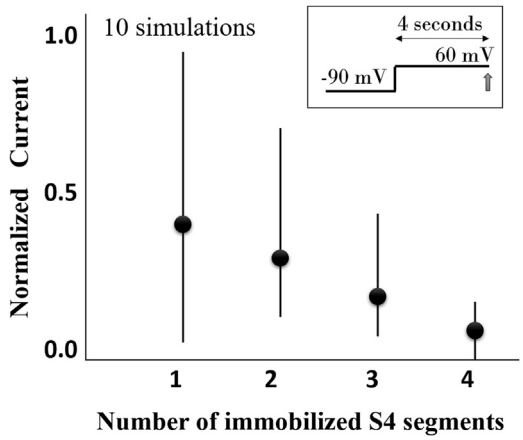

FIGURE 7 Sequential movement of S4 governs IKs gating. Using an alternative structure clustering method, an increasing number of S4 segments were prevented from moving upward during depolarization to 60 mV. The resulting current is measured 4 s postdepolarization (protocol in the *inset*). The plot shows a linear decrease of current with increasing number of immobilized S4 segments. Ten simulations were performed for each combination of S4 suppression. For example, two immobilized S4 segments could either be on adjacent or opposite sides of the tetramer. The 10 simulations for each of the possible S4 suppression combinations yielded the current mean (*filled circle*) and the minimum and maximum (error bars) of the plotted values. The results were normalized to the control (simulation of current without S4 movement suppression). The large variance is due to dissimilarity in ionic current reduction depending on whether proximal or distal S4 was immobilized.

vary. Therefore, we assumed that S4 *Z* translation across the membrane contributes most to changes in fluorescence, with smaller effects due to rotation or *X*, *Y* translation. In support of this assumption, the computed sum of four S4 *Z* displacements (Fig. 4) was consistent with experimental fluorescence data (10). As in experiments, simulated macroscopic current showed slower rise relative to S4 *Z*, indicating that S4 *Z* movement leads pore ion conduction (Figs. 4 and 5). Simulations show that initial movements of S4 and pore, because of depolarizing V_m, result in conformations with low or nonconducting SC. Therefore, little to no current is observed at first. With time, as IKs transitions to higher S4 Z and larger PD, higher SC levels are accessed, resulting in a larger current.

Other IKs fluorescence experiments also show two distinct fluorescence-voltage components (F1 and F2): F1 representing the large and fast IKs movements at negative V_m and F2 the smaller and slower component measured at positive V_m, respectively (31,32). These experiments also showed that the second structural IKs movement (represented by F2) correlated with significant increase in current. Therefore, in agreement with a concerted gating model, it was proposed that F1 and F2 components represented S4 activation and pore opening, respectively (7,10). However, this IKs gating model could not account for SCs reported by IKs single-channel recordings and had to be modified to include conductance levels for different numbers of activated S4 in the tetramer (9). Our model is consistent with the latter premise that with increasing number of activated VS, IKs can access larger SC states. However, our model does not reproduce the rapid transitions of IKs from large SC to nonconducting states. We believe that these transitions are caused by extrinsic SC factors that are not represented in this model, e.g., number and location of ions in the pore, ion hydration, van der Waals interactions between ions, water and pore residues, presence of nonpotassium ions in the pore, etc.

IKs conformational trajectories after depolarization

Fig. 5 (*right*) identifies important structural clusters and major conformational pathways (groups of trajectories) upon depolarization from −80 to 60 mV and −40 mV. The pink pathway encompasses mostly S4 *Z* translations, and the green and blue pathways include pore expansion. These pathways were identified by analyzing trajectories from each starting HPSS clusters to high SC clusters. Hit probabilities (transition probability between identified clusters) show that very few deeply closed conformations (small pore and low S4 *Z*) transition to high SC clusters upon depolarization (*blue*). Interestingly, 78% of total structures occupy this small-pore, low-S4-*Z* cluster at −80 mV. Very few IKs channels occupy the pink cluster and thus contribute very little to current upon depolarization. Nevertheless, this trajectory is responsible for the initial current increase. Approximately 18% of conformations occupy the green cluster and contribute to current rise later in time. As expected, the probability of transitioning to high SC clusters is smaller at −40 mV than at 60 mV. The pathways used to calculate hit probabilities are the major structural transitions that contribute to ionic current during IKs activation. As a model-based inference, we suggest that these pathways are closely related to experimentally detected current activation time constants, i.e., the fast and slow time constants correspond with pink and green pathways in Fig. 5, respectively.

S4 movement and pore opening

Similar to S4 *Z* upward movement, the pore follows an independent time course of opening. Hit probabilities (Fig. 5, *right*) show that the pathway of mostly S4 upward movement (*pink*) was much more probable than other pathways (*green* and *blue*). The pathway that required the largest PD increase (*blue*) to reach high SC states was least probable. Thus, initial Avg.S4Z transition (from −10 to ∼1 Å) was much faster than the second Avg.S4Z transition (from ∼1 to 3 Å), which in turn was faster than pore opening. A cartoon in Fig. 6 (*right*) explains these dynamics further.

Using kernel density estimation (KDE) of occupied structure clusters at SS for a range of V_m between −80 and 60 mV

helped identify important cluster groups that were visited upon depolarization (Fig. 6, *left*). Temporal KDE data (Fig. 5, *top*) show that conformations experiencing step depolarization to negative V_m undergo only the first fast transition (I), in which the dynamics are mostly determined by upward S4 *Z* translation (from −8 to ∼1 Å). For positive depolarization to V_m, conformations initially experience the first transition, followed by a second slower transition (II) of small S4 *Z* movement (from ∼1 to 3 Å) and medium to large PD increase, consistent with experimental data (10). The VS two-step transitions correlate with the fast (I) and slow (II) transitions of S4 (Fig. 4). Ionic current follows S4 movement with a delay because pore opening is slow compared to S4 *Z* transitions.

The third, much slower transition (III), from very small to large pore, involves small S4 *Z* movement (from ∼1 to 3 Å) that occurs at positive V_m and takes a much longer time. Consequently, IKs channels take a very long time to reach SS. This provides a likely explanation for the experimentally observed IKs current increase over very long times postdepolarization.

For one iCh, I contributes most to GC displacement. II, at positive V_m, involves a very small S4 *Z* translation and therefore contributes much less to GC displacement. As V_m increases, more iCh transition to conformations with higher S4 *Z*, as reflected in the sum shown in Fig. 4 (*red*). However, for one iCh, the S4 *Z* movement is small and contributes minimally to GC, which exhibits saturation (Fig. 4, *blue*).

Our structurally based model of IKs shows similar characteristics to the Zaydman-Cui kinetic (Markov) IKs model (32); the movement "I" (resting to intermediate state transitions) confers little to no current in both models. It follows that our structure-based model can be correlated to the Zaydman-Cui kinetic model that represents simplified transitions from resting to intermediate and intermediate to activated states. The correspondence requires a small modification to the Zaydman–Cui model of IKs; instead of suppressing transitions from intermediate-closed to intermediate-open states in the presence of KCNE1, the intermediate-open and activated-open states could be associated with very small and large conductances, respectively. This adjustment will enable transitions between intermediate-open and activated-open states, vital for IKs activation in our structure-based model. With this modification, the resting, intermediate and activated kinetic states can be associated with Avg.S4 Z conformations less than −5 Å, between −5 and ∼1.2 Å and greater than ∼1.2 Å, respectively. Also, we suggest that the Zaydman-Cui model of KCNQ1 could be modified with similar adjustments, but with a reduced difference between intermediate-open and activated-open conductances to account for its smaller SC range. The Zaydman-Cui model suggests that the functional VS-pore coupling is reduced in IKs relative to KCNQ1. Our structure-based model of IKs supports this supposition, as transitions to intermediate conformations result in extremely small current, and transitions to activated states are required for substantial increase in current.

Residue interactions that govern S4 *Z* movement

IKs conformational changes, in the presence of V_m, depend largely on the environment of charged S4 residues. Fig. S17 *A* shows a cartoon depicting S4 charged residues as well as the surrounding charged residues in the VS domain (S1–S4) and KCNE1 TM segment. Interaction strength between residue pairs and contribution of individual charged S4 residues to protein stabilization show that proximal and distal S4 undergo two types of movement based on their proximity to KCNE1. Distal S4 is likely to move upward faster than proximal S4 upon depolarization (Fig. S17 *B*) because strong interactions between proximal S4 and KCNE1 slow S4 transitions from low to high *Z* positions, resulting in slow activation (Fig. 17 *C*). Charged KCNE1 residues (R67, K69, K70, and E72) interact strongly with proximal S4 residues and have weaker interactions with distal S4 residues. These KCNE1 residues contribute most to proximal S4 stabilization at low *Z* through their interactions with R243 and D242 residues. Distal S4 is likely to be stabilized at ∼1 Å after depolarization and is unlikely to transition further in the *Z* direction. However, proximal S4 (although slower), can transition to higher S4 *Z* positions (∼3 Å). Ensemble VS movement has an initial large transition (fast) followed by a smaller *Z* transition (slow). The second ensemble S4 movement, observed at positive V_m (Fig. 4), is likely the result of proximal S4 transitioning from intermediate-to-high *Z* positions. The first ensemble S4 movement is possibly a combination of fast distal S4 (low-to-high) and slow proximal S4 (low-to-intermediate) *Z* transitions. In both proximal and distal S4, R228 plays an important role in stabilizing S4 at high *Z* positions.

Sequential gating

The simulations show that macroscopic current increases linearly with increasing number of moving S4 segments (Fig. 7). This is because IKs SC depends on all four S4 and pore conformations. High SC conformations are only accessible when all four S4 move to high *Z* positions with large PD. Nonetheless, small and intermediate SC conformations are accessible at low S4 *Z* with medium-to-large PD. The IKs pore is not tightly coupled to S4 *Z* movement because of the flexible S4-S4S5L three-residue segment (QGG; an additional ∼25° flexibility compared to Kv1.2/2.1 (33)). Thus, IKs pore openings (with small or intermediate SC conformations) are possible at lower S4 *Z* conformations. Large pore opening is most probable with all four S4 at high *Z*. Structurally, the pore can open (increase in diameter) at low-to-medium S4 *Z* positions, but the model IKs does not present with significant current until S4 *Z* reaches

relatively high positions. Consequently, from a model-based inference, we suggest that IKs gating is structurally allosteric but functionally concerted.

CONCLUSIONS

The methodology presented here is a computational framework for studying, through simulations, the atomistic interactions and dynamics of a protein that govern its biological function. The framework is applicable to most proteins and is a powerful tool for understanding protein behavior. This methodology can also be applied to study the effects of mutations, ligands, and drugs. Additionally, IKs structural and functional changes during an AP can be examined (34,35).

The structural model (Fig. 1) is not based on the recently published cryo-EM data of KCNQ1 structure bound to calmodulin (CaM) (33). This cryo-EM structure presents close homology to Kv1.2/2.1 TM segments and is very similar to the initial IKs structure in our library, with some differences in the intracellular domain. In particular, our model presents a different S6-HelixA attachment and number (three in Cryo-EM versus two in model) of Ca ions bound to CaM. The framework presented here allows incorporating these features into future structural libraries for evaluation of their effects on gating. We estimate that contribution to IKs energy will be minimal, as CaM is in the water/ion medium. Also, the presence of KCNE1 in our structures (but not in the cryo-EM structure) is an important feature of human IKs, as it could restrict pore opening.

The presented model uses implicit dielectrics to represent membrane and water/ion surfaces. Thus, it is possible that important van der Waals interactions between the protein and membrane that affect gating could have been underestimated. However, given that IKs C-terminus extends over 60 Å, explicit calculations would slow the computation 200-fold. With future advances in computational hardware and algorithms, it will likely be possible to incorporate an all-atom energy calculation as part of the gating model. In this study, protein dynamics was coarse-grained (by clustering structures) but was sufficiently fine to replicate all experimental data. The resolution can be tuned, based on study requirements, by increasing the number of structure clusters and random walks.

SUPPORTING MATERIAL

Supporting Materials and Methods. Supporting Results, and eighteen figures are available at http://www.biophysj.org/biophysj/supplemental/S0006-3495(18)30469-7.

AUTHOR CONTRIBUTIONS

S.R. performed the simulations and analyzed data. Y.R. supervised the project and analyzed data. Both authors conceived the project and wrote the manuscript.

ACKNOWLEDGMENTS

The authors are grateful to Prof. Bernard Attali, Tel Aviv University, for providing experimental data.

This study was supported by National Institutes of Health–National Heart, Lung, and Blood Institute grants R01-HL-033343 and R01-HL-049054 (to Y.R.). Y.R. is the Fred Saigh Distinguished Professor at Washington University. Computations were performed using facilities in the Rudy Lab and Washington University Center for High-Performance Computing, which is partially supported by National Center for Research Resources grant 1S10RR022984-01A1.

REFERENCES

1. Murata, K., and M. Wolf. 2018. Cryo-electron microscopy for structural analysis of dynamic biological macromolecules. *Biochim. Biophys. Acta.* 1862:324–334.
2. Rudy, Y., and J. R. Silva. 2006. Computational biology in the study of cardiac ion channels and cell electrophysiology. *Q. Rev. Biophys.* 39:57–116.
3. Rudy, Y. 2012. Mathematical modeling of complex biological systems: From genes and molecules to organs and organisms: heart. *In* Comprehensive Biophysics. E. H. Egelman, ed. Elsevier, pp. 268–327.
4. Jensen, M. O., D. W. Borhani, …, D. E. Shaw. 2010. Principles of conduction and hydrophobic gating in K+ channels. *Proc. Natl. Acad. Sci. USA.* 107:5833–5838.
5. Silva, J. R. 2018. How to connect cardiac excitation to the atomic interactions of ion channels. *Biophys. J.* 114:259–266.
6. Banyasz, T., Z. Jian, …, Y. Chen-Izu. 2014. Beta-adrenergic stimulation reverses the I Kr-I Ks dominant pattern during cardiac action potential. *Pflugers Arch.* 466:2067–2076.
7. Silva, J., and Y. Rudy. 2005. Subunit interaction determines IKs participation in cardiac repolarization and repolarization reserve. *Circulation.* 112:1384–1391.
8. Omichi, C., Y. Momose, and S. Kitahara. 2010. Congenital long QT syndrome presenting with a history of epilepsy: misdiagnosis or relationship between channelopathies of the heart and brain? *Epilepsia.* 51:289–292.
9. Werry, D., J. Eldstrom, …, D. Fedida. 2013. Single-channel basis for the slow activation of the repolarizing cardiac potassium current, IKs. *Proc. Natl. Acad. Sci. USA.* 110:E996–E1005.
10. Barro-Soria, R., S. Rebolledo, …, H. P. Larsson. 2014. KCNE1 divides the voltage sensor movement in KCNQ1/KCNE1 channels into two steps. *Nat. Commun.* 5:3750.
11. Meisel, E., M. Dvir, …, B. Attali. 2012. KCNQ1 channels do not undergo concerted but sequential gating transitions in both the absence and the presence of KCNE1 protein. *J. Biol. Chem.* 287: 34212–34224.
12. Nekouzadeh, A., and Y. Rudy. 2016. Conformational changes of an ion-channel during gating and emerging electrophysiologic properties: application of a computational approach to cardiac Kv7.1. *Prog. Biophys. Mol. Biol.* 120:18–27.
13. Nekouzadeh, A., and Y. Rudy. 2011. Continuum molecular simulation of large conformational changes during ion–channel gating. *PLoS One.* 6:e20186.
14. Nekouzadeh, A., J. R. Silva, and Y. Rudy. 2008. Modeling subunit cooperativity in opening of tetrameric ion channels. *Biophys. J.* 95:3510–3520.
15. Silva, J. R., H. Pan, …, Y. Rudy. 2009. A multiscale model linking ion-channel molecular dynamics and electrostatics to the cardiac action potential. *Proc. Natl. Acad. Sci. USA.* 106:11102–11106.
16. Webb, B., and A. Sali. 2014. Protein structure modeling with MODELLER. *Methods Mol. Biol.* 1137:1–15.

17. Baker, N. A., D. Sept, …, J. A. McCammon. 2001. Electrostatics of nanosystems: application to microtubules and the ribosome. *Proc. Natl. Acad. Sci. USA.* 98:10037–10041.

18. Callenberg, K. M., O. P. Choudhary, …, M. Grabe. 2010. APBSmem: a graphical interface for electrostatic calculations at the membrane. *PLoS One.* 5:e12722.

19. Buitinck, L., G. Louppe, …, G. Varoquaux. 2013. API design for machine learning software: experiences from the scikit-learn project. *arXiv*:1309.0238, https://arxiv.org/abs/1309.0238.

20. Best, R. B., X. Zhu, …, A. D. MacKerell. 2012. Optimization of the additive CHARMM all-atom protein force field targeting improved sampling of the backbone φ, ψ and side-chain χ1 and χ2 dihedral angles. *J. Chem. Theory Comput.* 8:3257–3273.

21. Hastings, W. K. 1970. Monte Carlo sampling methods using Markov chains and their applications. *Biometrika.* 57:97–109.

22. LLC Schrödinger. 2015. The PyMOL Molecular Graphics System, Version 1.8..

23. Darden, T., D. York, and L. Pedersen. 1993. Particle mesh Ewald: an N.log(N) method for Ewald sums in large systems. *J. Chem. Phys.* 98:10089–10092.

24. Yang, Y., and F. J. Sigworth. 1998. Single-channel properties of IKs potassium channels. *J. Gen. Physiol.* 112:665–678.

25. Biscani, F., D. Izzo, and M. Maertens. 2017. esa/pagmo2: pagmo 2.5. In Zenodo.

26. Haitin, Y., and B. Attali. 2008. The C-terminus of Kv7 channels: a multifunctional module. *J. Physiol.* 586:1803–1810.

27. Chapman, M. L., and A. M. VanDongen. 2005. K channel subconductance levels result from heteromeric pore conformations. *J. Gen. Physiol.* 126:87–103.

28. Nango, E., A. Royant, …, S. Iwata. 2016. A three-dimensional movie of structural changes in bacteriorhodopsin. *Science.* 354 (6319):1552–1557.

29. Howard, R. J., V. Carnevale, …, B. S. Rothberg. 2018. Permeating disciplines: overcoming barriers between molecular simulations and classical structure-function approaches in biological ion transport. *Biochim. Biophys. Acta.* 1860 (4):927–942.

30. Sesti, F., and S. A. Goldstein. 1998. Single-channel characteristics of wild-type IKs channels and channels formed with two minK mutants that cause long QT syndrome. *J. Gen. Physiol.* 112:651–663.

31. Osteen, J. D., C. Gonzalez, …, R. S. Kass. 2010. KCNE1 alters the voltage sensor movements necessary to open the KCNQ1 channel gate. *Proc. Natl. Acad. Sci. USA.* 107:22710–22715.

32. Zaydman, M. A., M. A. Kasimova, …, J. Cui. 2014. Domain-domain interactions determine the gating, permeation, pharmacology, and subunit modulation of the IKs ion channel. *eLife.* 3:e03606.

33. Sun, J., and R. MacKinnon. 2017. Cryo-EM structure of a KCNQ1/CaM complex reveals insights into congenital long QT syndrome. *Cell.* 169:1042–1050.e9.

34. O'Hara, T., L. Virág, …, Y. Rudy. 2011. Simulation of the undiseased human cardiac ventricular action potential: model formulation and experimental validation. *PLoS Comput Biol.* 7:e1002061.

35. Clancy, C. E., and Y. Rudy. 1999. Linking a genetic defect to its cellular phenotype in a cardiac arrhythmia. *Nature.* 400:566–569.